



HAL
open science

Micron-sized dust and nanoparticles produced in the WEST tokamak

C Arnas, A Campos, M Diez, Samuel Peillon, C Martin, K Hassouni, A Michau, E Bernard, N Fedorczac, Francois Gensdarmes, et al.

► **To cite this version:**

C Arnas, A Campos, M Diez, Samuel Peillon, C Martin, et al.. Micron-sized dust and nanoparticles produced in the WEST tokamak. Nuclear Materials and Energy, 2023, 36, pp.101471. 10.1016/j.nme.2023.101471 . hal-04086324v2

HAL Id: hal-04086324

<https://hal.science/hal-04086324v2>

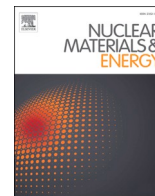
Submitted on 20 Jul 2023

HAL is a multi-disciplinary open access archive for the deposit and dissemination of scientific research documents, whether they are published or not. The documents may come from teaching and research institutions in France or abroad, or from public or private research centers.

L'archive ouverte pluridisciplinaire **HAL**, est destinée au dépôt et à la diffusion de documents scientifiques de niveau recherche, publiés ou non, émanant des établissements d'enseignement et de recherche français ou étrangers, des laboratoires publics ou privés.



Distributed under a Creative Commons Attribution 4.0 International License



Micron-sized dust and nanoparticles produced in the WEST tokamak

C. Arnas^{a,*}, A. Campos^b, M. Diez^c, S. Peillon^d, C. Martin^a, K. Hassouni^e, A. Michau^e,
E. Bernard^c, N. Fedorczac^c, F. Gensdarmes^d, C. Grisolia^c, B. Pégourié^c, E. Tsitroné^c

^a CNRS, Aix-Marseille université, PIIM, 13397 Marseille, France

^b Aix-Marseille université, CNRS, Centrale Marseille, FSCM, CP2M, 13397 Marseille, France

^c IRFM/CEA Cadarache, 13108 St Paul Lez Durance, France

^d LPMA/IRSN, 91192 Gif-sur-Yvette, France

^e LSPM, CNRS, Université Paris 13, Sorbonne Paris Cité, 93430 Villetaneuse, France

ARTICLE INFO

Keywords:

WEST
Tokamak dust
W nanoparticle
He nanobubble

ABSTRACT

Two populations of dust particles were found during the first phase of operation of WEST. The one that dominates by size and weight comes from the delamination of tungsten coatings covering graphite tiles and the emission of droplets of molten materials during off-normal events. Sizes vary from several microns to tens of microns. More generally, micron-sized dust particles due to the erosion of all materials present in the vacuum vessel were collected. In addition, nanocavities were found at the surface of tungsten dust sampled after He plasmas and were attributed to He trapping in the form of nanobubbles. Tungsten nanoparticles constitute the second unexpected dust population. They are dominant by their number and were essentially found at the surface of micron-sized particles. They may result either from the condensation of an oversaturated vapor above molten tungsten or come from ion-neutral clusters growing in plasma regions of low temperature until the appearance of solid particles.

Introduction

Plasma-wall interaction is at the origin of several varieties of dust particles. In ITER for which the divertor will be made of tungsten (W) and the first wall of beryllium (Be), they will be tritiated, activated, chemically reactive and toxic. Hence, during an accidental opening, a risk of environment contamination must be considered [1–3]. This potential issue will depend on the produced quantities and adhesion forces on plasma facing components (PFCs) [4–6]. In addition to safety risks, their presence could reduce the expected performances. W dust mobilization during plasma operation can be a source of high-Z contamination of the core plasma and tritium retention in dust deposits could impact the efficiency of the fuel cycle. It is therefore important to explore all the production possibilities. Literature reports that in current tokamaks of metallic PFCs, dust particles are mainly produced by off-normal events as arcing identified in ASDEX upgrade (AUG) [7–9], VDE and disruptions identified in JET, FTU, also in AUG and Alcator C-Mod [10–12]. The general effect is to melt the metal inducing emission of liquid droplets [13,14]. As they are easily deformable, they can be converted into spheroid dust particles before solidification or form

liquid splashes on PFCs [12–15].

In this paper, we present examples of dust particles produced during the two last plasma campaigns of the first phase of operation of WEST (C4-2019 and C5-2020). This study is complementary to analyses of thin and thick deposits made after the same plasma campaigns on the lower divertor of WEST [16–18]. The goal of all these investigations is to give information on the consequences of wall erosion in a metallic tokamak. Hence, two dust populations have been found: i) dust particles of several microns to tens of microns attributed to off-normal events as spheroids resulting from metal droplet emission and small pieces of delaminated W coatings and, ii) not expected in tokamak of W-PFCs, nanoparticles (NPs) of smallest sizes ~ 5 nm. Carbon NPs were also found in tokamaks of graphite-based PFCs, in particular in TEXTOR [19], Tore Supra [20] and MAST [21]. Comparisons with NPs produced in laboratory plasmas were also reported [19,22]. The proposed assumption on the formation mechanism was a growth mode resulting from successive specific collisions between eroded species, leading to nucleation and solid particles. With metallic PFCs, nucleation in oversaturated vapor above molten metal may also be considered [23].

In the micron size range, dust particles with surface nanocavities

* Corresponding author.

E-mail address: cecile.arnas@univ-amu.fr (C. Arnas).

have also been found after the C4 plasma campaign. The last two weeks of C4 being dedicated to study He plasma-wall interaction, these nanocavities have been attributed to He trapping in the form of He nanobubbles [24–27]. Examples will be presented and discussed considering WEST parameters [28].

Experiments

C4 and C5 plasma campaigns in WEST

WEST is a tokamak dedicated to testing the actively-cooled ITER-like W divertor in steady state plasmas [29]. During the first phase of operation (2016–2020), one of the 12 toroidal sectors of the lower divertor was progressively equipped with ITER-like plasma facing units (PFUs) as shown Fig. 1. Some of them were pre-damaged and vertically misaligned to investigate the produced damages under plasma exposure [30,18]. All other sectors of the lower divertor consisted in carbon-based tiles with 15 μm W coating called inertial PFUs. Some of them were equipped with additional Mo and W layers to be used as erosion markers. Fig. 1 shows a part of the toroidal vessel with 14 ITER-like PFUs (red square) specific of the C4 plasma campaign (2019) operating in the L mode. The outer limiter was made of W bulk tiles and the six inner bumpers were 15 μm W coated graphite tiles. The baffle consisted of 15 μm W coated CuCrZr components. There were ~ 135 min of D plasmas with 13 boronizations. The end of C4 was dedicated to ~ 45 min of He plasmas without boronization. The heating power varied from 0.5 to 8 MW (combining lower hybrid to ion cyclotron resonance heating) and the plasma current, from 0.2 to 1 MA. During C5 (2020), two sectors were equipped with ITER-like PFUs (a total of 76 PFUs). The central parts of the outer limiter and inner bumpers were replaced by low Z tiles made of BN. There were ~ 40 min of D plasmas in L mode and three boronizations. The heating power varied from 0.5 to 6 MW and the plasma current from 0.3 to 0.8 MA. There was a large number of disruptions during both plasma campaigns (>2000 disruptions).

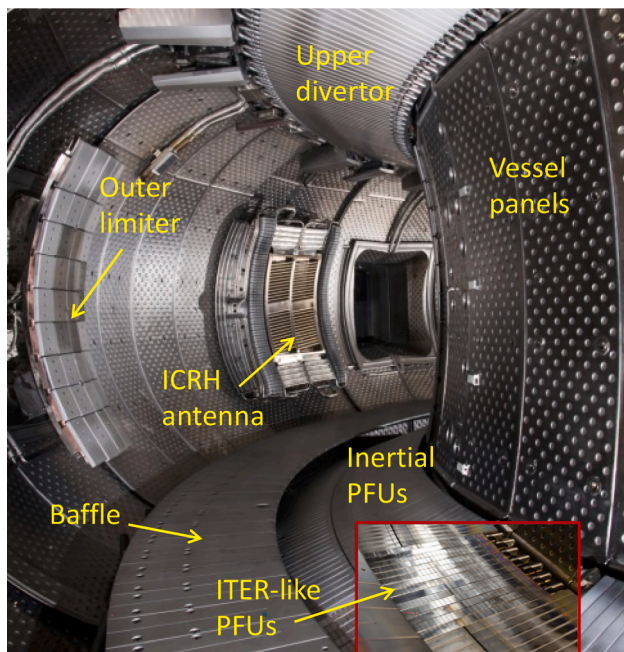


Fig. 1. WEST vacuum vessel during C4 showing: the lower divertor with 14 W ITER-like PFUs (red square) and the rest of W coated graphite PFUs or inertial PFUs, the baffle of W coated Cu fingers, an ICRH antenna with Ag protection, the upper divertor of W coated Cu tiles and the inner stainless-steel wall. (For interpretation of the references to colour in this figure legend, the reader is referred to the web version of this article.)

Dust collection procedure and diagnostics

After venting the vacuum vessel and a safety control, dust collection was performed on the lower divertor using the filtered vacuum technique. A small oil-free vacuum pump (ARICA 6VK) of 7 m^3/h influx without load was put on a safety platform set under an open port of the tokamak. It was connected to a hand-held filter holder by means of a plastic tube of ~ 10 m long. The filter holder has a plastic nozzle of ~ 0.2 cm in diameter. It was loaded with specific thin filters of 4.7 cm in diameter containing holes of controlled sizes of 0.4 μm . For dust collection, the nozzle of the filter holder was in contact with the surfaces of the investigated PFCs. As there was no guarantee that all surfaces were fully or homogeneously scanned, the dust weight was not measured and qualitative measurements were mainly favored. Four successive sectors were investigated (Q2A/Q2B and Q3A/Q3B) for the two plasma campaigns, C4 and C5. After C4, only one filter was used for all ITER-like PFUs (Q3B sector) and another one for inertial PFUs of the same sector. Three filters were used for the other three sectors (Q2A, Q2B, Q3A). During C5, as the entire sector Q3B was equipped with ITER-like PFUs, one filter was used for each sector: the sector facing an ICRH antenna (shown Fig. 1, sector Q2B), the sector equipped with inertial PFUs covered with successive W and Mo coatings used as erosion markers (Q2A), the sector of the outer limiter (Q3A) and the sector of ITER-like PFCs (Q3B).

For analyses, filters were pressed towards microscope holders of diameter ~ 1 cm, covered with double-sided adhesive carbon tapes and dust particles were transferred to them. This sensitive operation could tear the filters because of their thin thickness and dust particles could be lost during the transfer. Analyses have shown that this operation could also break thin dust particles coming from delaminated W coatings. Characterizations were made using an ultra-high resolution field emission Scanning Electron Microscope (Zeiss Gemini 500 - SEM) coupled to an energy dispersive X-ray spectroscopy (EDS) detector (SDD EDAX). Secondary electrons (SE) images were performed to study morphologies and sizes. Magnifications used in most cases were as high as possible to find nanoparticles. With an incident electron beam energy of 10–15 kV, these images have revealed the dust topography slightly below the dust surface, at a depth of 10–15 nm. The option “in lens” that allows to detect SE electrons directly in the beam path was also used. Hence, being surface sensitive especially at low kV, this option allowed to image the dust surface and comparison with layers of materials below the surface was possible. Backscattered electrons (BSE) were collected to highlight different chemical compositions by means of contrast variations on a given dust particle or between various particles. In particular, in BSE images (also in SEM images but not as much), heavy elements as W, Mo appear bright and light elements, dark as for B and C.

Choice of dust particles to show

It quickly became obvious that comparisons of dust as a function of the location for a given plasma campaign or as a function of the plasma campaign for a given location were going challenging. The general trend is that all materials present in the vacuum vessel in addition to W (C, Cu, Ag, Mo, Fe, Cr, Ni, Al...) can generate dust particles either separately or in the form of dust of mixed materials (also with W) or appear as traces. Their diversity comes from the inner wall which is made of stainless steel (Fe, Cr, Ni, Co); Faraday shields of ICRH antennas consist on Cu coated with Ag; LH antennas are Cu; the upper divertor and baffle tiles are Cu covered with W coating; tiles of inertial PFUs and protections of antennas are C-based with Mo/W coatings and interlayers of some inertial PFUs are Mo used as erosion marker. Other impurities as B and N injected respectively, before plasma operation for wall conditioning and during plasmas for radiating properties [31,32] were also found. O coming mainly from native oxide of all metals in the vacuum vessel, observed during plasma operation [33–35] and from the air exposure after plasma operation was found in all the analyzed dust particles. Dust

coming from outside the vessel made of Si, K, Ca, Mg... or human activities as textile fibers were also present.

In a first approach, microparticles and nanoparticles produced during C4 and C5 will be presented indifferently as no specificity was found linked to the plasma campaign and due to the presence everywhere of W, major element of interest in plasma-wall interaction. Moreover, analyses have revealed that in the micron size range, dust particles can be transported out of their region of production during off-normal events. By contrast, the presence of nanocavities at the dust surface observed after C4 will be specifically correlated to He plasmas produced at the end of this plasma campaign.

Micron-sized dust particles due to off normal events

Dust particles in the size range of several microns to tens of microns are essentially attributed to off normal events. In addition to spheroid, most of them have irregular shapes and surface roughness and come from the delamination of W coatings. They can be mixed to other materials or just contain traces of these materials.

Fig. 2 shows the analysis of a dust particle of size $\sim 50 \mu\text{m}$ coming from inertial PFUs (C4 campaign). The EDS spectrum reveals the presence of W and impurities as B, C, O and the four colored mappings give the distribution of each of these chemical elements. W in yellow and O in blue are present in the same areas (all bright parts of SEM image) and indicate that W appears in the form of oxide. B in red is present irregularly on some dark parts and shows that this dust particle was partially boronized. C in green appears on other dark parts in addition of the adhesive carbon tape where the particle was stuck. These traces of C are

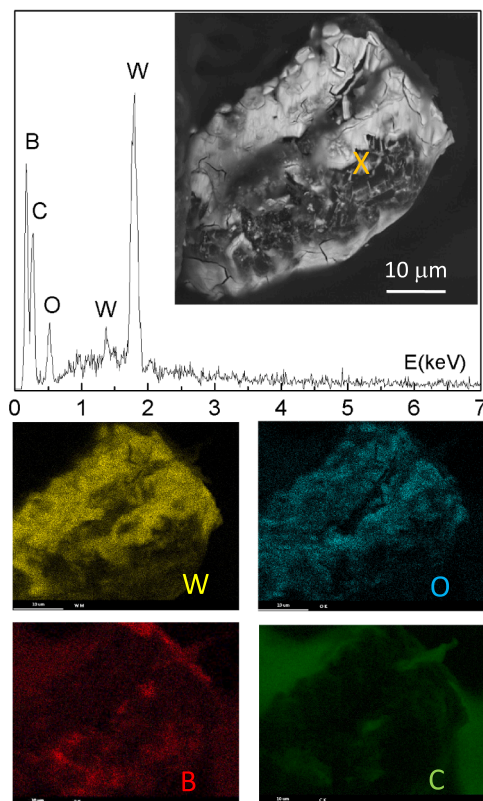


Fig. 2. SEM image of a dust (top right) coming from inertial PFUs, size $\sim 50 \mu\text{m}$ (C4 campaign); presence of W, B, C and O in the EDS spectrum collected on the orange cross area. Colored mappings of the same chemical elements: W (in yellow) is oxidized (O in blue); B (in red) is present in some dark parts of SEM image; C (in green) appears on other dark parts and the carbon adhesive tape around. (For interpretation of the references to colour in this figure legend, the reader is referred to the web version of this article.)

consistent with the erosion of graphite tiles after W coating delamination observed directly on inertial PFUs [36].

Fig. 3 a) shows several W dominated particles collected on ITER-like PFUs (C4 campaign). They have very different shapes and surface roughness, and sizes varying roughly between ~ 4 and $\sim 9 \mu\text{m}$. Magnification of the bottom three particles is shown Fig. 3 b) with three colored EDS spectra corresponding to areas of each of them (colored crosses). In addition to the presence of W and C, there are traces of B, N, O and also Cu, depending on the dust particle. If surface structures are now considered, the dust particle of the right side (Fig. 3 b)) has the characteristics of columnar deposits consisting of tapered units separated with voids. In the corresponding deposition mechanism, the incident particle flux is preferentially deposited at the top of surface irregularities due to limited diffusion and shadowing effects [37,38]. The left dust particle has a very heterogeneous surface consisting of smooth parts and irregular holes. Both features reveal an initial molten surface where boiling could occur, generating vapor and producing cavities. The dust of fairly smooth surface at the image bottom seems to be made of several layers of deposited W. There is also at the top right side of Fig. 3 a) a spheroid, characteristic of a molten W droplet after solidification.

All the above-mentioned features suggest that the dust particles of Fig. 3 can come from any area of ITER-like PFUs but also from different locations in the vacuum vessel. In particular the spheroid particle could come from the outer limiter (not far from ITER-like PFUs), camera having shown that this component emits droplets after disruption. Cracks and melting of the poloidal edges of vertically misaligned ITER-like PFUs have also been observed with sometimes stuck W droplets [36]. The three dust particles at the top left side of Fig. 3 a) seem to be small pieces of W coating, consistent with the proximity of inertial PFUs where W coating was delaminated [36]. Therefore, the plasma exposure of graphite tiles after delamination can explain the presence of C in all spectra of Fig. 3 b). Moreover, the presence of columnar deposits is consistent with thick and rough deposits that were observed on the high field side of ITER-like PFUs [16,36].

Other dust particles correlated to PFU damage are presented Fig. 4 and are typical of W droplets emitted during off normal events. Fig. 4 a) shows a spheroid of $\sim 6 \mu\text{m}$ collected on the sector of inertial PFUs with interlayers of Mo and W used for erosion investigation (C5 campaign). EDS spectrum shows mainly W in the composition and O (likely W oxide). There are also traces of Mo revealing that the interlayers of Mo were reached and eroded in accordance with their direct observation on PFUs [17,36]. Traces of C may be attributed again to graphite tile erosion during plasma exposure. SEM image also shows that projections of molten W (mainly on the left side) were made on the spheroid dust of temperature close to that of a solid (no merging with W projections). Fig. 4 b) shows another spheroid of $\sim 5 \mu\text{m}$ coming from ITER-like PFUs (C4 campaign). Dark areas on most of the surface are B (dominant B line on EDS spectrum) and small bright parts are W. These features suggest that this dust particle was mainly W and was boronized after being deposited.

Dust particles without W but consisting sometimes of complex metal mixtures were found after C4 and C5. This is illustrated Fig. 5 where sizes vary from several μm to tens μm . The dust of Fig. 5 a) is Cu with traces of Mo, C and O, and comes from inertial PFUs. Fig. 5 b) is a mixture of Ag and Mo with traces of C, O and Cu. It was found in the sector of an ICRH antenna. The particle of Fig. 5 c) is stainless steel (Fe, Ni, Cr, Co, O). Fig. 5 d) shows two pieces of B coating of $>400 \mu\text{m}$ long. The dust particle of Fig. 5 e) found on inertial PFUs is essentially C with traces of O.

Nanoparticles and discussion on their origins

NPs have been essentially observed at the surface of micron-sized dust particles at high SEM magnification. They have various characteristics giving clues on the formation and growth mechanisms that will

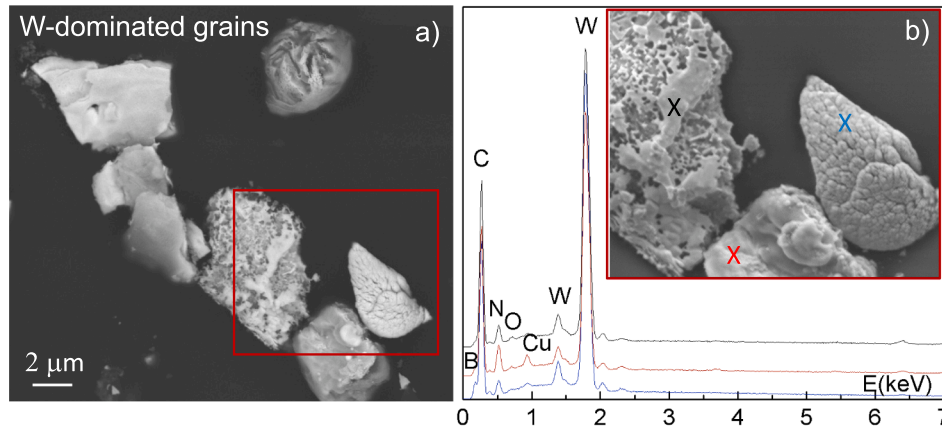


Fig. 3. a) W dust particles of various shape and surface roughness (C4 campaign); b) details of the three dust particles in the red square. Three superimposed EDS spectra give the chemical composition of each of them (colored crosses). In addition to W and C, there are traces of B, N, O and Cu. (For interpretation of the references to colour in this figure legend, the reader is referred to the web version of this article.)

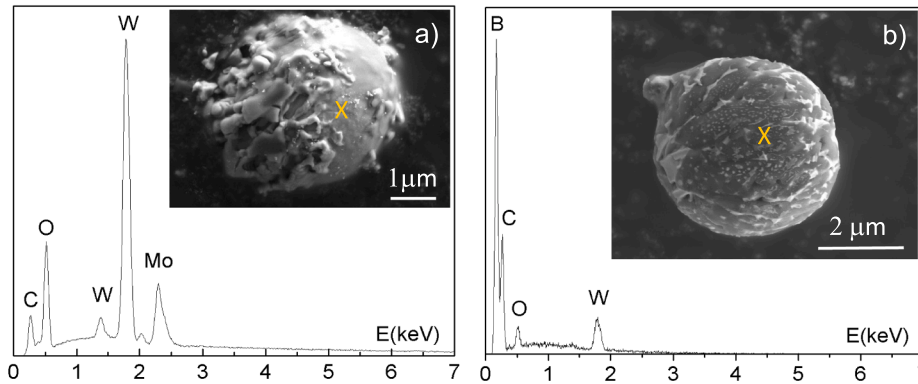


Fig. 4. a) W dominated spheroid containing C, O and Mo traces, size $\sim 6 \mu\text{m}$ (C5 campaign). Molten W projections on the left side indicate that the dust temperature was close to that of a solid; b) B dominated spheroid containing C, O traces, size $\sim 5 \mu\text{m}$ (C4 campaign). It was likely W before boronization.

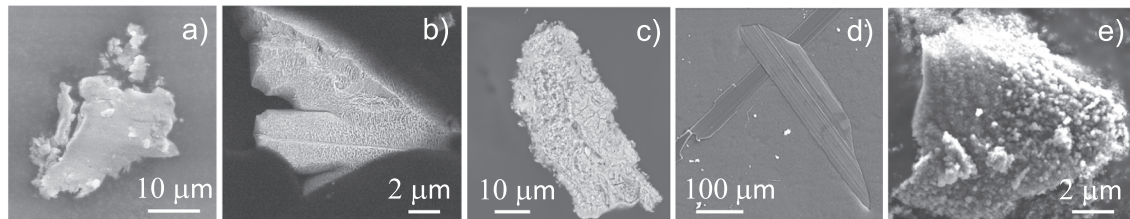


Fig. 5. Dust particles of complex shapes and mixtures; a) Cu particle with traces of Mo, C and O; b) mixture of mainly Ag and Mo with traces of C, O and Cu; c) stainless-steel dust; d) two pieces of B coatings; e) C dust with traces of O.

be discussed.

Fig. 6 a) shows a piece of W coating of $\sim 27 \mu\text{m}$ long and $\sim 8 \mu\text{m}$ wide coming from inertial PFUs after C4. Examples of NPs in two different areas of the upper part (red and green squares) are shown Fig. 6 b)-c). In both cases, they are dispersed and have similar sizes, from ~ 8 to ~ 23 nm. More information is given Fig. 6 d) (blue square of Fig. a)). In the left side, dispersed NPs are deposited on a smooth area. The right part is characterized by a strong surface roughness. This difference of roughness as well as the presence of a narrow smooth bulge between both areas may indicate that the left side was likely melted and vaporized and a part of the vapor could be deposited on the right side. If we assume that NPs present above the smooth area are the result of this microparticle surface structure evolution as a function of time, they may have been formed by condensation of W vapor after its cooling (nucleation in

oversaturated vapor) [23,39,40]. Another possibility could be a nucleation from specific ion-neutral collisions until the appearance of NPs also mentioned when NPs were observed in tokamaks with graphite-based PFCs [19,22].

Fig. 7 a) shows a dust particle found on inertial PFUs after C4, resulting from the merging of two W droplets, each one of $\sim 2 \mu\text{m}$ in size. NPs are present everywhere on the surface. The magnification of the red square shows a population of ~ 20 nm average size and few bigger ones (Fig. 7 b)). The same pathways of formation as for Fig. 6) may be considered here.

Fig. 8 a) shows a dust of $\sim 90 \mu\text{m}$ long and $\sim 40 \mu\text{m}$ wide collected on the sector of ITER-like PFUs (C5 campaign). EDS spectra (not shown here) of dark parts reveals a dominant contribution of B with the presence of W and O, and also traces of C, N and Cu. Fig. 8 b) shows the

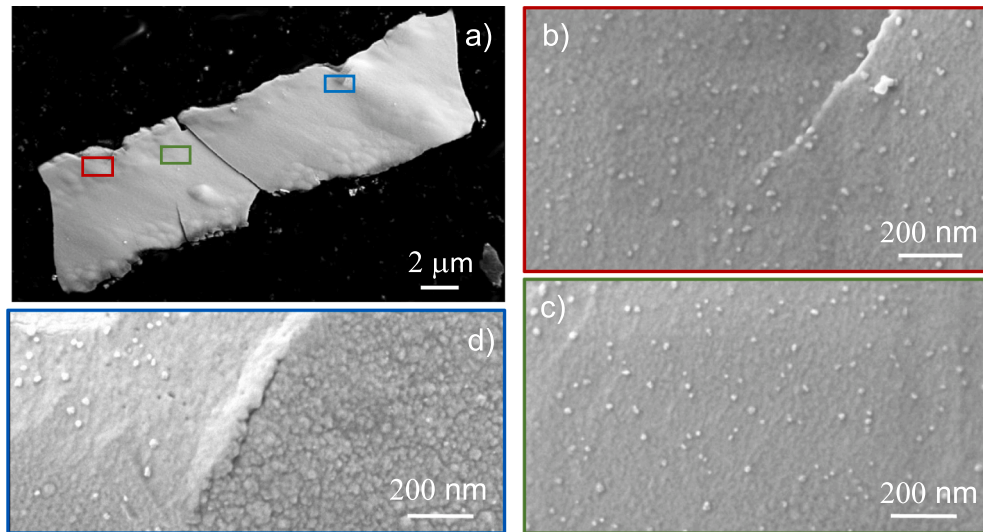


Fig. 6. a) piece of W coating of $\sim 27 \mu\text{m}$ long and $\sim 8 \mu\text{m}$ wide (C4 campaign); b) and c) magnifications of the red and green squares of a) showing dispersed NPs of similar sizes, from 8 to 23 nm; d) detail of the blue square showing a smooth W area (left part) with dispersed NPs and a rough W area (right part). (For interpretation of the references to colour in this figure legend, the reader is referred to the web version of this article.)

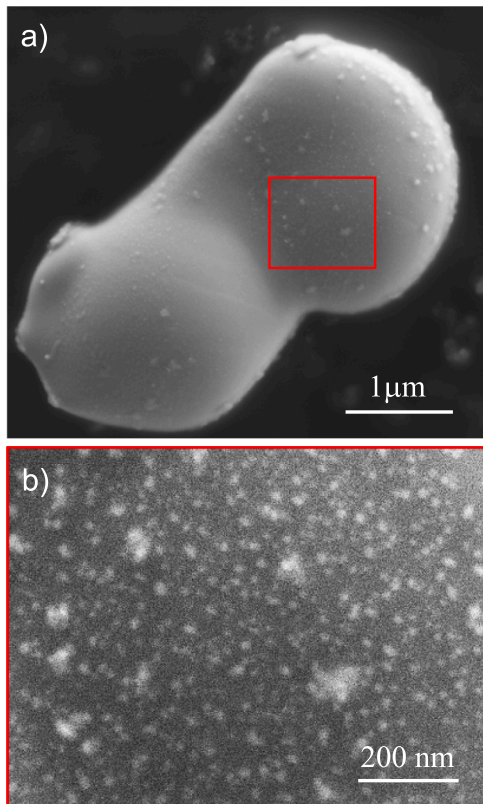


Fig. 7. a) two merged W droplets of size $\sim 2 \mu\text{m}$ each one (C4 campaign). NPs are present everywhere on the surface; b) magnification of the red square showing NPs of $\sim 20 \text{ nm}$ average size and few bigger ones. (For interpretation of the references to colour in this figure legend, the reader is referred to the web version of this article.)

magnification of a bright part (red square) in Fig. 8 a). The background is made of dispersed NPs of $\sim 5 \text{ nm}$. There are also larger particles (largest size $\sim 50 \text{ nm}$) either separated or melted with others to form chains shown with yellow arrows. All these features reveal that the dust of Fig. 8 a) is a small piece of W coating that was boronized; then, NPs were deposited on it after boronization and likely after delamination.

Fig. 8 c) shows another bright part (black square in Fig. 8a)). NPs of $\sim 5 \text{ nm}$ are still in the background with others of larger sizes in the range of 10–15 nm. The latter are either separated or agglomerated to form bigger particles as illustrated in yellow circles. The fact that they are still visible indicates that their initial temperature was lower than the melting temperature. This suggests that the agglomeration process was made between neutral NPs after the plasma termination or between solid NPs of fluctuating charges during plasma operation. Studies in low temperature plasmas have indeed shown that the presence of NPs of negative, neutral and positive charges enhances the agglomeration mechanism [41–43].

He nanobubbles at the dust surface

Fig. 9 a) shows a small piece of W coating of $\sim 5 \mu\text{m}$ in length, collected on ITER-like PFUs after C4. SEM images have revealed the presence of nanoholes all over the surface. The

average size on the dust tip (Fig. 9 b)) deduced from the measured size distribution (inset) is 10.9 nm and the standard deviation is 3.4. Fig. 9 c) is a magnification of the red square of Fig. 9 a). Fig. 9 d) shows the same area but with a focus of the microscope electron beam allowing to explore the dust surface while in Fig. 9 c), the microscope electron beam adjustment allowed to probe 10–15 nm below the surface (see Section 2.2 for explanations). This procedure has revealed the presence of domes at the exact position of nanoholes and therefore, made it possible to highlight the presence of nanocavities. The latter have been attributed to He nanobubble formation during the two last weeks of C4 dedicated to He plasmas.

The goal of He plasmas during C4 was to investigate W structure changes under He irradiation. The parameters of the outer strike point regions of the lower divertor were in the range of those required to generate nanofibers, the so-called W fuzz as highlighted in linear plasma devices with relevant parameters for fusion plasmas. The latter have explored the formation of He bubbles [24–27] as well as the growth of W fuzz from He bubbles [44–46]. It was shown that both W structure changes are produced with complex parameter mixtures as the incident ion energy E_{He^+} , fluence and W temperature. For instance, nanobubbles were produced in laboratory experiments with $E_{\text{He}^+} = 250 \text{ eV}$, a fluence $< 10^{21} \text{ He}^+/\text{m}^2$ and a maximum W temperature of 1073 K [24]. In WEST, measurements with Langmuir probes gave $E_{\text{He}^+} > 20 \text{ eV}$ leading to 150–300 eV energies on the outer strike point surface, and large accumulated fluence ($> 10^{24} \text{ He}^{++}/\text{m}^2$). A temperature $> 700 \text{ }^\circ\text{C}$ was

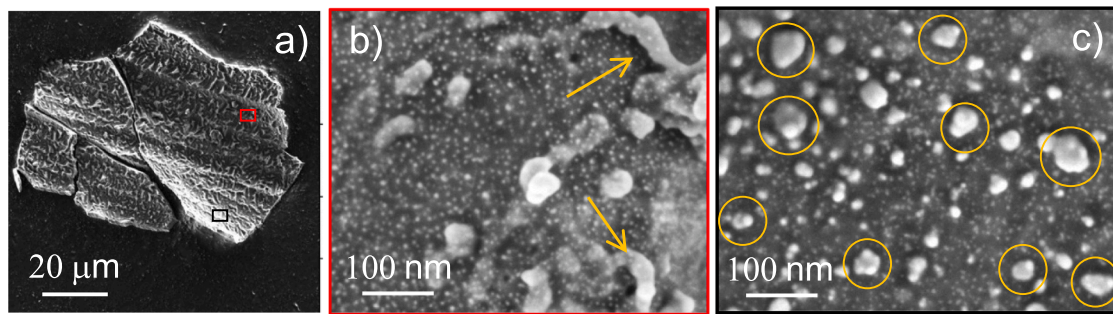


Fig. 8. a) piece of W coating of $\sim 90 \mu\text{m}$ long and $\sim 40 \mu\text{m}$ wide (C5 campaign); b) details of a whitish part made of dispersed NPs of $\sim 5 \text{ nm}$ in the background (red square). Larger ones are either separated or melted with others to form chains (arrows); c) another whitish part (black square) still showing NPs of $\sim 5 \text{ nm}$ in the background and bigger ones either separated or agglomerated (yellow circles). (For interpretation of the references to colour in this figure legend, the reader is referred to the web version of this article.)

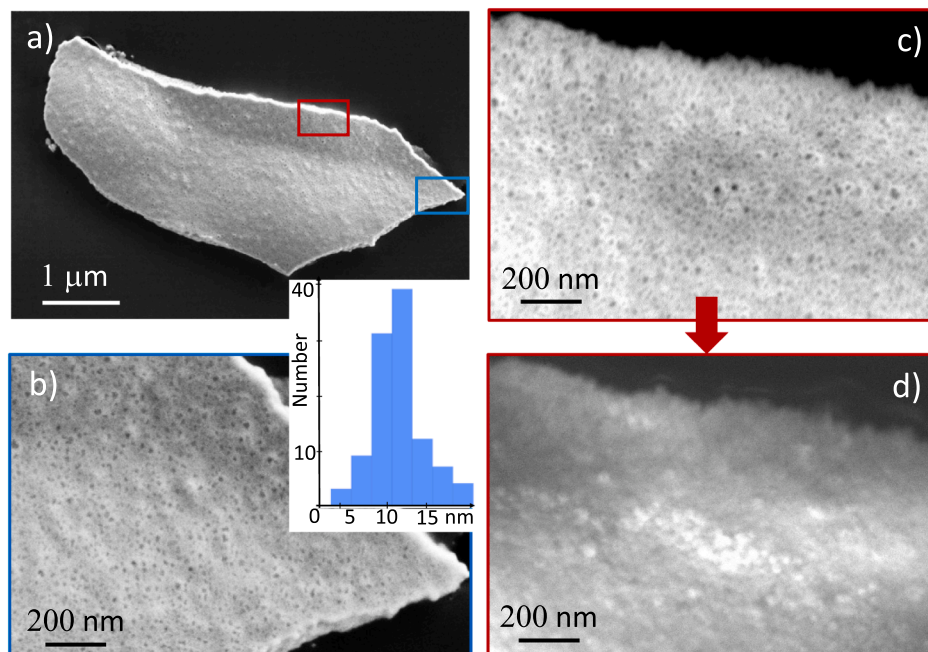


Fig. 9. a) piece of W coating of $\sim 5 \mu\text{m}$ long with nanoholes all over the surface (C4 campaign); b) size distribution (inset) of nanoholes of the dust tip; average size of 10.9 nm ; c) nanoholes in the red square of a); d) same area as c) revealing the presence of domes at the exact position of nanoholes in c), highlighting the presence of nanocavities produced by He nanobubbles. (For interpretation of the references to colour in this figure legend, the reader is referred to the web version of this article.)

deduced from IR measurements [28,47]. More details can be found in the reference E. Tsitroni *et al* [28] about these parameters as well as discussions on their choice. In particular, it is indicated that due likely to a competition between W fuzz growth and W erosion by impurities not present in controlled laboratory experiments, and due to temperatures not constant on the strike point regions during plasma pulses, W fuzz was not produced. However, the parameters may have been favorable for He bubbles formation on some locations. Moreover, similar nanoholes as those of Fig. 9. b) have been found after C4, on thick W dominated deposits collected near the inner strike point [16]. As the piece of W coating of Fig. 9 was transported from inertial PFUs to ITER-like PFUs and due to the inhomogeneity of the parameters of strike point regions, it is not possible to evaluate the formation conditions. However, their presence everywhere on the surface with similar sizes indicates at least, homogeneous incident parameters at the dust scale.

Conclusion

Two classes of dust particles were found in the WEST tokamak after

the plasma campaigns of C4 (2019) and C5 (2020). The one that dominates by size and weight is due to off-normal events. They can produce dust coming from the delamination of W coatings of inertial PFUs as well as emission of droplets of molten W and all materials present in the vacuum vessel giving rise to dust of spherical and irregular shapes. As all inertial PFUs of the lower divertor were recently replaced with ITER-like PFUs, the number of dust particles due to delamination is expected to decrease significantly during all future plasma campaigns. In addition, nanocavities of homogeneous sizes were observed at the surface of W micron-sized particles produced during C4. The end of this plasma campaign being dedicated to He plasmas, their presence has been attributed to He trapping in the form of nanobubbles. W nanoparticles which are dominant by their number constitute the second dust population. They were found for the first time in a metallic tokamak essentially at the surface of micron-sized particles. Two main pathways may be considered for their formation, either from the condensation of an oversaturated vapor above molten W surface or from specific ion-neutral collisions. In the latter case, the growth of ion metallic clusters may be considered either in initial W vapor or in regions of low plasma

temperature fed with W sputtering.

CRedit authorship contribution statement

C. Arnas: Investigation, Methodology, Writing – original draft. **A. Campos:** Methodology. **M. Diez:** Methodology, Resources. **S. Peillon:** Methodology. **C. Martin:** Methodology. **K. Hassouni:** Validation. **A. Michau:** Validation. **E. Bernard:** Validation. **N. Fedorczak:** Validation. **F. Gensdarmes:** Validation. **C. Grisolia:** Supervision. **B. Pégourié:** Validation. **E. Tsitrone:** Supervision.

Declaration of Competing Interest

The authors declare that they have no known competing financial interests or personal relationships that could have appeared to influence the work reported in this paper.

Data availability

No data was used for the research described in the article.

Acknowledgments

This work has been carried out within the framework of the EUROfusion Consortium, funded by the European Union via the Euratom Research and Training Programme (Grant Agreement No 101052200 - EUROfusion). Views and opinions expressed are however those of the author(s) only and do not necessarily reflect those of the European Union or the European Commission. Neither the European Union nor the European Commission can be held responsible for them.

References

- [1] M. Shimada, R.A. Pitts, S. Ciattaglia, S. Carpentier, C.H. Choi, G. Dell Orco, T. Hirai, A. Kukushkin, S. Lisgo, J. Palmer, W. Shu, E. Veshchev, J. Nucl. Mater. 438 (2013), <https://doi.org/10.1016/j.jnucmat.2013.01.217>. S996-S1000.
- [2] C. Grisolia, F. Gensdarmes, S. Peillon, G. Dougniaux, E. Bernard, A. Autrique, G. Pieters, B. Rousseau, S. Feuillastre, S. Garcia-Argote, C., Uboldi et al Nuc. Fus. 59 (2019), 086061, <https://doi.org/10.1088/1741-4326/ab1a76>.
- [3] S. Peillon, G. Dougniaux, M. Payet, E. Bernard, G. Pieters, S. Feuillastre, S. Garcia-Argote, F. Gensdarmes, C. Arnas, F. Miserque, N. Herlin-Boime, C. Grisolia, O. Pluchery, Nuc. Mater. Energy 24 (2020), 100781, <https://doi.org/10.1016/j.nme.2020.100781>.
- [4] S. Ratynskaia, P. Toliás, M. De Angeli, V. Weinzettl, J. Matejicek, I. Bykov, D. L. Rudakov, L. Vignitchouk, E. Thorén, G. Riva, D. Ripamonti, T. Morgan, R. Panek, G. De Temmerman, Nucl. Mater. Energy 12 (2017) 569, <https://doi.org/10.1016/j.nme.2016.10.021>.
- [5] A. Rondeau, J. Merrison, J.J. Iversen, S. Peillon, J.C. Sabroux, P. Lemaitre, F. Gensdarmes, Fus. Engin. Design 98–99 (2015) 2210, <https://doi.org/10.1016/j.fusengdes.2014.12.038>.
- [6] L. Vignitchouk, K. Paschalidis, S. Ratynskaia, P. Toliás, R.A. Pitts, Plasma Phys. Control. Fusion 65 (2023), 015014, <https://doi.org/10.1088/1361-6587/aca827>.
- [7] V. Rohde, M. Balden, T. Lunt, the ASDEX Upgrade team., Phys. Script. T138 (2009), 014024 DOI 10.1088/0031-8949/2009/T138/014024.
- [8] M. Balden, N. Endrasser, P. Humrickhouse, V. Rohde, M. Rasinski, U. von Toussaint, S. Elgeti, R., Neu and the ASDEX Upgrade team, Nucl. Fusion 54 (2014), 073010 DOI 10.1088/0029-5515/54/7/073010.
- [9] F. Brochard, V. Rohde, T. Lunt, G. Suarez Lopez, A. Shalpegin, R. Neu, ASDEX Upgrade team, Nucl. Mater. Energy 18 (2019) 268 10.1016/j.nme.2019.01.014.
- [10] E. Fortuna-Zalesna, J. Grzonka, M. Sunwoo Moon, P. Rubel, A.W. Petersson, J.E. T. Contributors, Phys. Scr. 217 (2017), 014038 DOI 10.1088/1402-4896/aa8ddf.
- [11] M. De Angelis, G. Maddaluno, L. Laguardia, D. Ripamonti, E. Perelli Cippo, M. L. Apicella, C. Conti, G. Giacomini, G. Grosso, J. Nucl. Mater. 463 (2015) 847 10.1016/j.jnucmat.2014.10.068.
- [12] C. Arnas, J. Irby, S. Celli, G. De Temmerman, Y. Addab, L. Couédel, C. Grisolia, Y. Lin, C. Martin, C. Pardanaud, S. Pierson, Nucl. Mater. Energy 11 (2017) 12, <https://doi.org/10.1016/j.nme.2017.02.027>.
- [13] A. Hassanein, I. Konkashbaev, J. Nucl. Mater. 283–287 (2000) 1171, [https://doi.org/10.1016/S0022-3115\(00\)00142-2](https://doi.org/10.1016/S0022-3115(00)00142-2).
- [14] B. Bazylev, G. Janeschitz, I. Landmana, A. Loartec, N.S. Klimov, V. L. Podkovyrov, V.M. Safronov, Fus. Eng. And Design 84 (2009) 441, <https://doi.org/10.1016/j.fusengdes.2008.12.123>.
- [15] L. Vignitchouk, A. Khodak, S. Ratynskaia, I.D. Kaganovich, Nucl. Mater. Energy 25 (2020), 100826, <https://doi.org/10.1016/j.nme.2020.100826>.
- [16] C. Martin, M. Diez, A. Campos, M. Cabié, G. Giacometti, M. Balden, A. Gallo, B. Pégourié, E. Bernard, E. Tsitrone, and the WEST Team, Phys. Scripta 96 (2021) 124035 DOI 10.1088/1402-4896/ac267e.
- [17] M. Balden, M. Mayer, B. Bliewert, E. Bernard, M. Diez, M. Firdaouss, M. Missirlian, B. Pégourié, M. Richou, H. Roche, E. Tsitrone, C. Martin, A. Hakola and the WEST Team, Phys. Scr. 96 (2021), 124020 DOI 10.1088/1402-4896/ac2182.
- [18] M. Diez, M. Balden, S. Bresinsek, Y. Corre, N. Fedorczak, M. Firdaouss, E. Fortuna, J. Gaspar, J.P. Gunn, A. Hakola, T. Loarer, C. Martin, M. Mayer, P. Reilhac, M. Richou, E. Tsitrone, T., Vuoriheimo and the WEST team, Nucl. Mat. Energy (2023), 10139910.1016/j.nme.2023.101399.
- [19] J. Winter, Plasma Phys. Control. Fusion 46 (2004) B583, <https://doi.org/10.1088/0741-3335/46/12B/047>.
- [20] P. Roubin, B. Pégourié, R. Smirnov, C. Martin, M. Richou, Y. Marandet, C. Pardanaud, C. Brosset, J. Gunn, J. Nucl. Mater. 390–391 (2009) 49, <https://doi.org/10.1016/j.jnucmat.2009.01.043>.
- [21] C. Arnas, C. Pardanaud, C. Martin, P. Roubin, G. De Temmerman, G. Counsell, J. Nucl. Mater. 401 (2010) 130, <https://doi.org/10.1016/j.jnucmat.2010.04.010>.
- [22] C. Arnas, C. Martin, P. Roubin, B. Pégourié, G. De Temmerman, K. Hassouni, A. Michau, G. Lombardi, X. Bonnin, Plasma Phys. Control. Fusion 52 (2010), 124007, <https://doi.org/10.1088/0741-3335/52/12/124007>.
- [23] J.P. Sharpe, B.J. Merrill, D.A. Petti, M.A. Bourham, J.G. Gilligan, J. Nucl. Mater. 290–293 (2001) 1128, [https://doi.org/10.1016/S0022-3115\(00\)00550-X](https://doi.org/10.1016/S0022-3115(00)00550-X).
- [24] H. Iwakiri, K. Yasunaga, K. Morishita, N. Yoshida, J. Nucl. Mater. 283–287 (2000) 1134, [https://doi.org/10.1016/S0022-3115\(00\)00289-0](https://doi.org/10.1016/S0022-3115(00)00289-0).
- [25] D. Nishijima, M.Y. Ye, N. Ohno, S. Takamura, J. Nucl. Mater. 329–333 (2004) 1029, <https://doi.org/10.1016/j.jnucmat.2004.04.129>.
- [26] E. Bernard, R. Sakamoto, A. Kreter, M.F. Barthe, E. Autissier, P. Desgardin, H. Yamada, S. Garcia-Argote, G. Pieters, J. Chêne, B. Rousseau, C. Grisolia, Phys. Scr. T170 (2017), 014023, <https://doi.org/10.1088/1402-4896/aa89f7>.
- [27] M. Ialovega, E. Bernard, M.-F. Barthe, R. Bisson, A. Campos, M. Cabié, T. Neisius, R. Sakamoto, A. Kreter, C. Grisolia, T. Angot, C. Martin, Nucl. Fusion 62 (2022), 126022, <https://doi.org/10.1088/1741-4326/ac94e3>.
- [28] E. Tsitrone, B. Pégourié, J.P. Gunn, E. Bernard, V. Bruno, Y. Corre, L. Delpêche, M. Diez, D. Douai, A. Ekedahl, N. Fedorczak, A. Gallo, T. Loarer, S. Vartanian, J. Gaspar, M. Le Bohec, F. Rigollet, R. Bisson, S. Brezinsek, T. Dittmar, G. De Temmerman, A. Hakola, T. Wauters, M. Balden, M. Mayer and WEST Team, Nucl. Fusion 62 (2022) 07602810.1088/1741-4326/ac2ef3.
- [29] J. Bucalosi, M. Missirlian, P. Moreau, F. Samaille, E. Tsitrone, D. van Houtte, T. Batal, C. Bourdelle, M. Chantant, Y. Corre, X. Courtois, L. Delpêche, L. Doceul, D. Douai, H. Dougnac et al, Fusion Eng. Des. 89 (2014) 907 10.1016/j.fusengdes.2014.01.062.
- [30] M. Richou, Y. Corre, T. Loewenhoff, M. Diez, C. Martin, A. Aretz, J. W. Coenen, M. Firdaouss, G. Giacometti, A. Grsjean, G. Pintsuk, H. Roche, M. Spahn, G. De Temmerman, E. Tsitrone, M. Wirtz and the WEST team, Nucl. Fusion 62 (2022) 05601010.1088/1741-4326/ac412e.
- [31] T. Loarer, T. Dittmar, E. Tsitrone, R. Bisson, C. Bourdelle, S. Brezinsek, J. Bucalosi, Y. Corre, L. Delpêche, C. Desgranges, G. De Temmerman, D. Douai, A. Ekedahl, N. Fedorczak, A. Gallo, et al., Nucl. Fus. 60 (2020), 126046 DOI 10.1088/1741-4326/abb919.
- [32] P. Maget, P. Manas, J.-F. Artaud, C. Bourdelle, J. Bucalosi, H. Bufferand, G. Ciraolo, C. Desgranges, P. Devynck, R. Dumont, N. Fedorczak, F. Felici, M. Göniche, C. Guillemaut, R. Guirlet, J.P. Gunn, T. Loarer, J. Morales, O. Sauter, S. Van Mulders, D., Vézinet and the WEST team, Plasma Phys. Control. Fusion 64 (2022), 045016 DOI 10.1088/1361-6587/ac4b93.
- [33] A. Gallo, A. Sepety, Y. Marandet, H. Bufferand, G. Ciraolo, N. Fedorczak, S. Brezinsek, J. Bucalosi, J. Coenen, F. Clairet, Y. Corre, C. Desgranges, P. Devynck, J. Gaspar, R. Guirlet, J. Gunn, C.C. Klepper, J.-Y. Pascal, P. Tamin, E. Tsitrone, E.a., Unterberg and the WEST team, Nucl. Fusion 60 (2020), 126048 DOI 10.1088/1741-4326/abb95b.
- [34] G.J. van Rooij, O. Meyer, S. Brezinsek, C. Desgranges, D. Douai, S. Ertmer, A. Gallo, C. Gil, J. Gunn, T. Loarer, E. Tsitrone, the EUROfusion PFC team and the WEST Team, Phys. Scripta T171 (2020), 014060, <https://doi.org/10.1088/1402-4896/ab606c>.
- [35] G. Ciraolo, S. Di Genova, H. Yang, A. Gallo, N. Fedorczak, H. Bufferand, J.P. Gunn, P. Tamin, R. Guirlet, C. Guillemaut, C. Desgranges, C. Bourdelle, E. Tsitrone, J. Bucalosi, M. S. d'Abusco, E. Serre, Y. Marandet, M. Raghunathan, A. Sepety, J. Romazanov, A. Kirschner, S. Brezinsek and the WEST Team, Nucl. Fusion 61 (2021) 126015 DOI 10.1088/1741-4326/ac2439.
- [36] M. Diez, Y. Corre, E. Delmas, N. Fedorczak, M. Firdaouss, A. Grosjean, J.P. Gunn, T. Loarer, M. Missirlian, M. Richou, E., Tsitrone and the WEST Team, Nucl. Fusion 61 (2021), 106011, <https://doi.org/10.1088/1741-4326/ac1dc6>.
- [37] J.A. Thornton, J. Vac. Sci. Technol. A 4 (1986) 3059, <https://doi.org/10.1116/1.573628>.
- [38] T. Karabacak, J.P. Singh, Y.-P. Zhao, G.-C. Wang, T.-M. Lu, Phys. Rev. B 68 (2003), 125408, <https://doi.org/10.1103/PhysRevB.68.125408>.
- [39] S. Panda, S.E. Pratsinis, NanoStructured Mater. 5 (1995) 755, [https://doi.org/10.1016/0965-9773\(95\)00292-M](https://doi.org/10.1016/0965-9773(95)00292-M).
- [40] R.C. Flagan, M.M. Lunden, Mater. Sci. and Engineering A204 (1995) 113, [https://doi.org/10.1016/0921-5093\(95\)09947-6](https://doi.org/10.1016/0921-5093(95)09947-6).
- [41] T. Matsoukas, M. Russel, J. Appl. Phys. 77 (1995) 4285, <https://doi.org/10.1063/1.359451>.
- [42] B.M. Annaratone, Y. Elskens, C. Arnas, T. Antonova, H.M. Thomas, G. Morfill, New J. of Physics 11 (2009), 103013, <https://doi.org/10.1088/1367-2630/11/10/103013>.
- [43] A. Michau, C. Arnas, K. Hassouni, J. Appl. Phys. 121 (2017), 163301, <https://doi.org/10.1063/1.4981245>.

- [44] M.J. Baldwin, R.P. Doerner, Nucl. Fusion 48 (2008), 035001, <https://doi.org/10.1088/0029-5515/48/3/035001>.
- [45] S. Kajita, N. Yoshida, R. Yoshihara, N. Ohno, M. Yamagiwa, J. Nucl. Mater. 418 (2011) 152, <https://doi.org/10.1016/j.jnucmat.2011.06.026>.
- [46] G. De Temmerman, K. Bystrov, J.J. Zielinski, M. Balden, G. Matern, C. Arnas, L. Marot, J. Vacc. Sci. Technol. A 041306201210 (1116/1) (2012) 4731196.
- [47] J. Gaspar, M.-H. Aumeunier, M. Le Bohec, F. Rigollet, S. Brezinsek, Y. Corre, X. Courtois, R. Dejarnac, M. Diez, L. Dubus, N. Fedorczak, M. Houry, V. Moncada, P. Moreau, C. Pocheau, C. Talatizi, E. Tsitrone, the WEST team, Nucl. Mater., Energy 25 (2020), 10085110.1016/j.nme.2020.100851.